A SIMULTANEOUS AND COUPLED SIMULATION SCHEME FOR THE CONVENTIONAL INTERMITTENT GAS LIFT

Clodoaldo de Oliveira Carvalho Filho
DEMP-UFC, P.Code 60455-760 , Fortaleza-CE
carvalho@dem.ufc.br

Sergio Nascimento Bordalo
DEP-FEM-UNICAMP, P.O.Box 6052, 13083-970, Campinas-SP
bordalo@dep.fem.unicamp.br

Abstract. The mechanistic models reported in the literature to describe the dynamics of the Conventional Intermittent Gas Lift (IGL) usually divide its operating cycle into five sequential and self-contained stages: injection, elevation, production, decompression and loading, restricting the system analysis to a limited range of operational conditions where such behavior is expected to happen. Evolving from those models, this paper proposes a new approach for the IGL simulation, where the well bore system is divided into two subsystems – comprising the well casing and the production tubing – coupled with the oil reservoir and the surface facilities throughout the entire IGL operating cycle, according to the proper boundary conditions and some special functions. This scheme extends the simulation capabilities to a wide range of operational conditions, including the off-design operation. In some cases, the simulation results show that some stages are in fact simultaneous and that considerable deviation from the sequntial operation may occur due to out-of-phase coupling. The coupled scheme for the IGL simulation improves the representation of the system dynamics, providing a valuable tool for the practice of the field engineer.

Keywords. *Artificial Lift, Intermittent Gas Lift, Petroleum Production, System Simulation*

1. Introduction

The intermittent gas lift (IGL) is a well-known artificial lift method used in the petroleum industry to produce oil wells when the reservoir is rather depleted or its productivity is too low to justify the utilization of a higher producing method. A high-pressure gas supply is used in the IGL to provide the supplement of energy necessary to lift the well liquids up to the surface. This method is able to produce within a wide range of flow rates and is particularly suitable to situations where the gas is available at low cost and can be dispensed to well clusters.

The IGL has some important variants, most of them fairly covered by the literature, but only the conventional arrangement will be considered here. A typical IGL-assisted well assembly is shown in Fig. (1) – it is a vertical well with the well casing and the inner production tubing. The casing annulus is sealed by a packer above the perforation section, forming a storage chamber for the high-pressure gas injected at the surface through the motor valve, usually operated in connection with a time controller (TC) for cyclic injection of gas according to predefined set points.

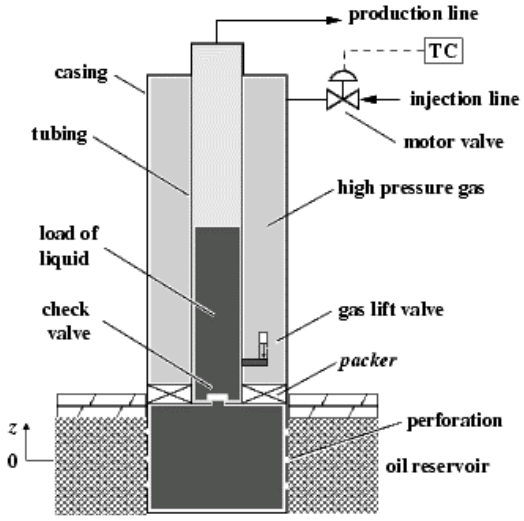

Figure 1. A typical IGL-assisted well assembly (the kick-off valves were intentionally omitted).

A gas-lift (GL) valve is located at some depth near the bottom of the annular space to permit the storage of gas and control its subsequent expansion into the tubing during the lift process. Two or more GL valves can be used for multi-point injection of the gas into the tubing, tough the conventional IGL generally uses only the lowest one in the normal operation. There is also a check valve at the bottom of the tubing to prevent the reverse influx of well liquids into the reservoir formation. As one may notice, the IGL-assisted well has the same down-hole equipment as the continuous gas-lift, used for more productive wells, so both methods are interchangeable with a few minor modifications.

The design and operation of the IGL must satisfy the requirement of profitable production – namely the highest oil production with a minimum gas consumption, thus the necessity for understanding the complex IGL behavior that emerges from its cyclic nature. In fact, the inefficiency and other problems attributed to the IGL may result from wrong design considerations or operation mistakes rather than from the method itself, leading to erroneous decisions in the field management and a consequent reduction of oil production profitability. Those situations clearly stress the importance of assessing the IGL behavior.

The early works of Brown and Jessen (1962), White et al. (1963), Brill et al. (1967) and Neely et al. (1973) described the IGL cycle through measurements on lab-tests and field wells. The cycle was divided into a number of stages, but the analysis was concentrated most on the lift process. The slug-flow pattern was observed during the upward travel of the liquid. The expanding gas was found to penetrate the slug of liquid above, apparently with a constant velocity, resulting on a so-called fallback of liquid into the gas phase – in the form of droplets and as a film on the tubing wall. Important conclusions about the recovery efficiency of the IGL were drawn relative to the effects of the GL-valve port size – it should be as large as practical, and relative to the liquid fallback – greater recovery are achieved increasing the amount of gas injected per cycle.

Semi-empirical models were derived to predict some parameters of the IGL behavior. Despite the simplicity and the adequacy of such models for handy calculations, most of them are based on results recorded just for the first cycle of the IGL operation, still under influence of transient effects. Indeed, they lack generality and lead to a fragmented analysis of the IGL behavior, since some aspects of its cycle remain unexposed.

Machado (1988) and Liao (1991) shifted the IGL modeling towards the application of the conservation laws of mechanics. The later author developed a comprehensive mechanistic model for the entire IGL cycle, obtaining results in good agreement with former experimental woks. He treated the IGL cycle as a sequence of 4 self-contained stages: lift of the slug of liquid in the tubing, production of the slug at the surface, production of liquid by entrainment and slug regeneration; deriving a complete set of ordinary differential equations for each one. The stages were simulated standalone through an iterative numerical procedure. Afterwards, Santos et al. (2001) extended the Liao's modeling approach to other variants of the IGL: with a chamber, with an ideal plunger and with a "pig"; also including the gas injection stage into the simulation.

Such an approach is expected to be more reliable than semi-empirical models since it is mainly grounded on general laws of physics. However, the mechanistic models still lack extensive field adjustment and validation, and its sophistication level reduces its applicability for practical field calculations (Chacín, 1994). Additional concern regards the division of the IGL cycle into sequential stages, since this pattern is supposed to exist only in a limited range of operational conditions. In fact, some of the depicted stages can superpose one another depending on operational parameters such as injection time and cycle period[1], leading to quite different results for the IGL outcome. Attempting to overcome the aforementioned drawbacks, this paper presents a new IGL model suited for coupled and simultaneous simulation of the entire IGL cycle.

2. Modeling of the IGL cycle

A new IGL model was developed based on Santos's mechanistic model, introducing special features to permit a coupled and simultaneous simulation of the IGL cycle. For simplicity, as the well overall performance results from the combined individual performances of the oil reservoir, the well bore and the surface facilities systems, the present model focused on the well bore, while the behavior of the other two systems was assumed as static (pressure) boundary conditions.

The well bore was split into 2 subsystems – comprising the casing annulus and the production tubing – and the IGL cycle divided into 5 stages: injection, elevation, production, decompression and loading. Those subsystems are connected to each other and to the other systems through valves and lines, so they can mutually interact throughout the entire operating cycle, according to proper boundary conditions. Depending on the subsystem, one or two distinct phases (liquid or gas) may flow within it. Each phase is represented by a control volume over which the conservative mass and momentum balances are applied. Constitutive relations are also needed to accomplish the description of the physical phenomena, such as state equations for real gases and correlations for fluid properties, friction factors, and mass flow rates through the valves.

From the IGL modeling emerges a complete set of 25 coupled time-dependent ordinary differential and algebraic equations, written in a general form as:

$$\frac{dE_j(Y)}{dt} - F_j(Y) = 0; \quad Y(t_o) = Y_o; \quad j = 1,\ldots,l \tag{1}$$

$$G_k(Y) = 0; \quad k = l+1,\ldots,n \quad (n = 25) \tag{2}$$

where Y is the vector of unknown variables y_i in Tab. (A.1) of Appendix A, and E, F and G are the real functions shown in Tab. (A.2-3). In addition, certain initial conditions must be known in advance to make the solution of Eq.(1) possible.

[1] Injection time is the time that the surface motor valve stands open for injection of gas into the casing annulus, and the cycle period is the time elapsed between two consecutive openings of the surface motor valve.

The current model introduces two remarkable improvements to the former mechanistic models:

- The film dynamics is determined by the momentum balance[2] along the entire IGL cycle, rather than by an empirical linear relation in terms of the slug velocity during the elevation and production stages;
- The same balance equations are valid throughout the entire IGL cycle due to the special functions that control the participation and the form of such equations during the simulation.

The special functions are logical expressions of integer flags that assume the values 0 or 1 according to the ongoing stage of the IGL cycle and the action of the valves, making the IGL model suitable for simultaneous simulation. The way the special functions work along the IGL cycle simulation will be explained in the next section.

3. Simultaneous and coupled simulation scheme

The mixed IGL equation set must be solved at every time-step, throughout the entire operation of the well, to simulate the IGL's dynamic behavior. In the course of the simulation, however, specific events in the IGL operation may lead to changes in the behavior of participating variables, thus letting some equations to be modified or completely removed from the simulation. Yet another equations can be added to keep both the physical and the mathematical consistency of the model. Furthermore, due to the cyclic nature of the IGL's behavior, it is often necessary to simulate a few cycles until a stationary regime is eventually reached, *i.e.* the cycles repeat themselves without noticeable changes on the IGL outputs.

Such a complexity requires a robust but simple simultaneous simulation scheme to perform successfully. The adopted scheme treats the IGL's dynamic behavior as a series of succeeding stationary states that evolve in time due to small perturbations in the overall system. The ordinary differential equations are made discrete in time through an implicit finite difference method, and the resulting non-linear algebraic equation set has to be solved by an iterative numerical procedure, *e.g.* the Newton-Raphson method, for each time-step. The dynamic simulation moves forward in time using the solution from one time-step as the initial condition for the next step of the simulation.

Departing from the sequential scheme of previous authors, the variables and equations concerning the 3 subsystems are not defined *a priori* for a single stage, but interactively settled across the ongoing stage of the IGL cycle. This scheme permits to identify and simulate situations where concurrent stages are taking place. For each time-step, the simulator checks the status of the integer flags, Tab. (B.1) of Appendix B, to determine what variables and equations are active, Tab(B.2-5), so the special functions can shape the form of the balance equations before they are passed to the solver. Another concern regarding to the solver is the varying number of variables and equations throughout the simulation. As fewer variables and equations remain active, the coefficient matrix of the Newton-Raphson simultaneous equation system tends to become sparse, impinging a computational burden for the solution procedure. To surmount this shortcoming, the solution procedure is carried out with the aid of auxiliary vectors used to store only the active elements of the system, thus eliminating the zero-elements of the original coefficient matrix. Such a procedure becomes interesting in face of the huge number of iterations to be performed during the entire simulation.

4. Applications of the simultaneous and coupled simulation scheme

To scrutinize the main features of the simultaneous and coupled simulation scheme, three typical cases of practical IGL application are considered. An IGL-assisted vertical oil well D_c = 139.7 mm (5 1/2 in) is perforated at H_{wh} = 1500 m – and produces 30º API oil with 50% of water in volume by the injection of gas d_g = 0.7 at P_{gi} = 7.85 Mpa. The well fluids are lifted against a wellhead pressure P_{wh} = 686.7 kPa through the production tubing D_t = 60.3 mm (2 3/8 in). A check valve is located at bottom of the tubing and one unbalanced and nitrogen-charged GL-valve is positioned 20 m above the check valve. The GL-valve geometry is resumed to the area ratio R = 0.26 and the seat diameter D_{gv} = 12.5 mm (1/2 in). For simplicity, the well packer is assumed to be at the GL-valve depth.

The well is equipped with a time-controlled motor valve at the surface so the injection time and the cycle period can be adjusted to control the IGL outcome according to reservoir and operational conditions for each case, shown in Tab. (1).

Table 1. Reservoir and operational conditions for the simulated cases.

Case	*PI* (m³/d/MPa)	h_s / H_{wh} (-)	h_{li} / h_s (-)	P_{vo} / P_{to} (-)	P_{gv} (MPa)	t_{inj} (s)	Δt_{cycle} (s)
#1: low *PI* and P_R	5	0.3	0.5	1.8	4.746	40.0	3,600.0
#2: low *PI* and high P_R	5	0.7	0.3	1.6	5.545	60.0	1,920.0
#3: high *PI* and low P_R	20	0.3	0.5	1.8	4.746	40.0	1,300.0

[2] New correlations are also used to evaluate the friction factor according to the two-phase flow relative motion.

The reservoir static pressure P_R and the initial load of liquid h_{li} are determined from the ratios between the static height h_s and the perforation depth H_{wh}., and the desired fraction of h_s to be lifted per cycle, respectively. The gas-charge of the GL-valve dome is established by h_{li}, the geometry of the valve and the opening casing-tubing pressure ratio P_{vo}/P_{to} that acts on both sides of the valve just before it opens. The three cases were simulated through the simultaneous and coupled scheme for 26,000 s and 0.1 s time-step. Despite of the numerical technique to be sensitive to the initial guesses, those simulations performed quickly and without convergence problems, attesting the robustness of the present scheme. In all cases, only the results for a stationary cycle were considered for analysis.

Observing the results for case #1, Fig. (2.a), one can see that the IGL cycle becomes almost stationary after the third cycle has been accomplished, when the volume of oil produced at the surface matches the volume fed by the reservoir, and the liquid fallback stabilizes at 14.3 %. Such transient behavior reinforces the belief that calculations based on the former semi-empirical models should be considered carefully, since they are based on first-cycle results.

The presence of fallback during the lift process is evidenced in Fig.(2.b). As the slug is lifted, its length – measured by the difference between the positions of the top of the slug z_s and the top of the gas core z_b – is progressively reduced due to the loss of liquid to the film on the tubing wall, since the liquid entrainment into the gas core is not considered in the present model. Fallback is speeded-up over the acceleration periods at the very beginning of the elevation and during the production stage, specially this one, due to the greater inertia of liquid. Although the gas core and slug velocities are not constant, the velocity of the gas penetration into the slug remains almost unchanged along those periods, as observed in the former experimental works.

The sequence of stages of the IGL cycle can be visualized through the action of three valves that connect the IGL subsystems in Fig. (2.c). Thirty-six seconds after the gas injection has begun – the motor valve status is "on" – the pressures acting on the GL valve, *i.e.* the gas pressure at the casing side P_{c2} and the hydrostatic pressure due to the liquid load at the tubing side P_{t1}, reach the P_{vo}/P_{to} ratio, see Fig. (2.d), and the valve opens – the GL-valve status is "on" – beginning the elevation stage. The tubing pressure below the slug builds up quickly and starts to decrease as soon as the gas injection ceases – the motor valve status is "off". The GL-valve remains open until P_{c2} becomes equal to P_{gv}, and then is closed – the GL-valve status is "off" – before the end of the production stage.

After producing the slug, an additional volume of liquid is also produced through the film dragged by the gas core, in the beginning of the decompression stage. In case #1, this volume was around 2.0 % of the total amount of liquid produced and somewhat compensates the neglected production through liquid entrainment. The IGL outcome for case #1 is shown in Fig. (2.e), resulting in 0.26 m³ (1.6 bbl) of oil per cycle with an injected gas-oil ratio IGOR of 520 m³/m³.

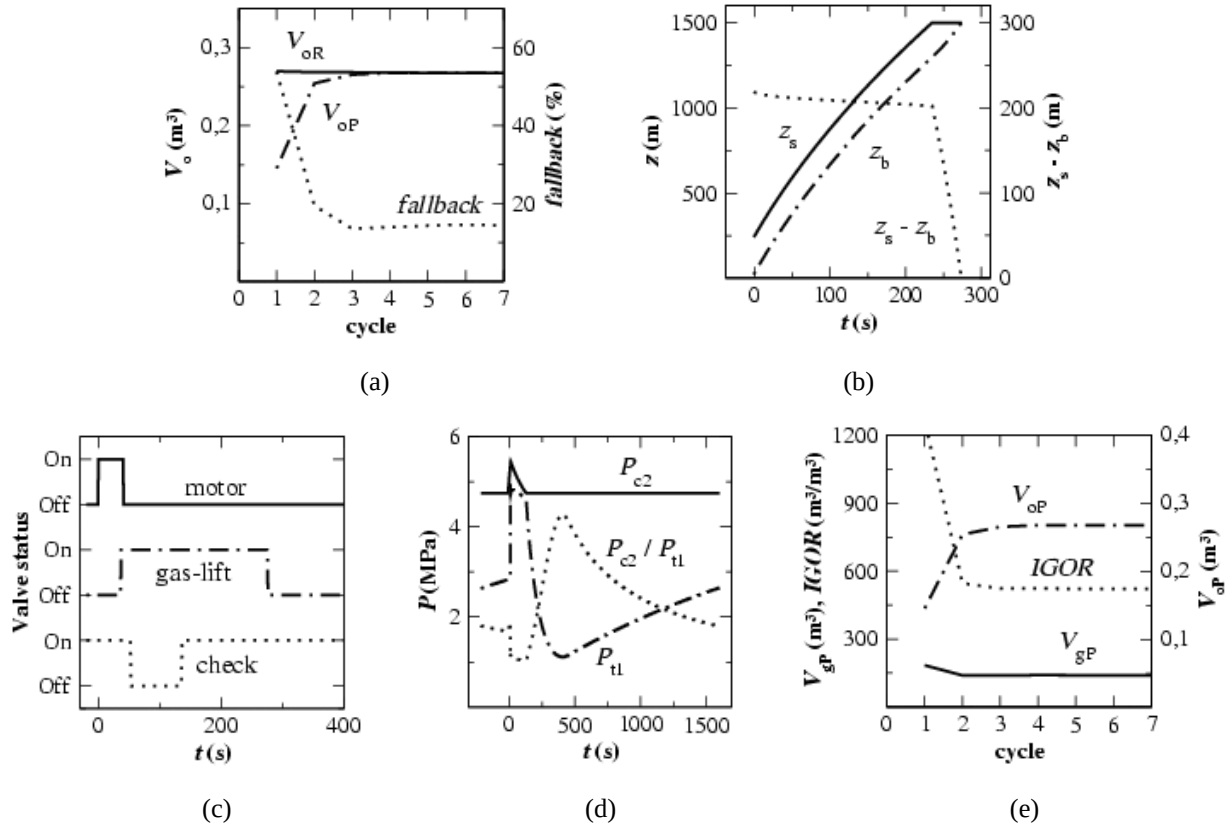

Figure 2. Simultaneous and coupled IGL simulation results for case #1: a) oil production and liquid fallback for several IGL cycles; b) positions of slug and gas core tops, and slug length during elevation and production; c) action of the valves for a stationary IGL cycle; d) pressures acting on the GL valve for a stationary IGL cycle; and e) gas consumption and oil production for several IGL cycles.

Other important observation regards to the behavior of the check-valve. There was a time lag between the opening of GL-valve and the time the check-valve closes – the check-valve status is "off" – early in the elevation stage. Within this interval, the reservoir static pressure was sufficient to keep the check-valve open and to feed oil into the well. The volume of oil fed during the period that the GL-valve remained open was incorporated to the film on the tubing wall. As P_{t1} decreases, the pressure difference across the check-valve kept the valve open – the check-valve status is "on" – still during the elevation stage, allowing the reservoir formation to produce into the well.

After the closure of the GL-valve, the liquid fed by the reservoir begun to accumulate at the bottom of the tubing string, restoring the liquid load to be lifted in the next IGL cycle. The falling film of liquid also led to a faster build up of the liquid load. Hence, the loading stage was superposed to the elevation and the subsequent stages. Such IGL behavior could not be evidenced by the previous sequential simulation schemes.

For case #2, a stabilization pattern was observed similarly to case #1. Once more superposing stages occurred in the IGL cycle. The GL-valve closed early in the decompression stage, indicating that an excessive amount of gas was injected on the current cycle, and the check-valve remained open throughout the entire cycle due to the high pressure of the oil reservoir. The size of the lifting slug increases early in the elevation stage, because of the incorporation of the falling film from the previous cycle, thus leading to a smaller fallback and a better *IGOR* as shown in Tab. (2).

The higher *PI* in case #3 resulted in a smaller cycle period for the IGL. The same observations for case #1 – regarding the stabilization and sequence of stages – hold in case #3, however, the fallback was smaller than in case #1, see Tab. (2). As the operational parameters for both cases are the same, except the cycle period, the smaller fallback indicates that the IGL outcome can be optimized for economical operation through careful adjustment of its parameters – the cycle period and injection time.

Table 2. The IGL outcome for the simulated cases.

Case	V_{op} (m^3)	*IGOR* (m^3/m^3)	Fallback (%)
#1	0.26	520.0	14.3
#2	0.40	498.4	8.2
#3	0.29	480.0	9.2

Although some of the features observed in the simultaneous and coupled simulation may be regarded as off-design IGL operation, they are likely to occur in the real field practice and must be considered consciously in the design and operation of the IGL wells.

5. Conclusion

This paper presented a new simultaneous and coupled scheme for the dynamic simulation of IGL operations through a mechanistic model. Such scheme accounts for the coupled operation of two interconnected subsystems – the casing annulus and the producing tubing – that interact with the oil reservoir and the surface facilities throughout the entire IGL cycle to produce the well liquids. Improvements regarding the momentum balance over the liquid film on the tubing wall and the use of special functions to control the behavior of model equation set through the entire IGL cycle were introduced to extend the simulation capabilities over a wider range of operational conditions.

Typical IGL applications for different combinations of reservoir parameters – *PI* and P_R – revealed that some of the IGL stages are simultaneous rather than sequential, depending on the adjustment of the cycle period and injection time. Such a departure from the sequential scheme may lead to different results concerning the IGL outcome and its optimal point of operation. Nevertheless, efforts must be directed to validate the IGL model against experimental and field data.

The simultaneous and coupled scheme may also be extended to other IGL variants as well, resulting on a valuable tool for the practitioner engineer to design IGL systems and to analyse their performance in field operation.

6. Acknowledgement

The authors would like to thank to Fundação Coordenação de Aperfeiçoamento de Pessoal de Nível Superior (CAPES), to Dept. of Mechanical Engineering of Universidade Federal do Ceará (DEMP-UFC) and to Dept. of Petroleum Engineering of Universidade Estadual de Campinas (DEP-FEM-UNICAMP) for the material and financial support to this work.

7. References

Brill, J.P., Doerr, T.C. and Brown, K.E., 1967, “An Analytical Description of Liquid Slug Flow In Small-Diameter Vertical Conduits”, Trans. AIME 240, JPT (SPE 1526), pp. 419-432.

Brown, K.E. and Jessen, F.W., 1962, “Evaluation of Valve Port Size, Surface Chokes and Fluid Fall-back in Intermittent Gas-Lift Installations”, Trans. AIME 255, JPT, pp. 315-322.

Chacín, J.E., 1994, “Selection of Optimum Intermittent Lift Scheme for Gas Lift Wells”, SPE 27986, pp. 301-313

Liao, T., 1991, “Mechanistic Modeling of Intermittent Gas Lift”, PhD thesis, U. of Tulsa, TX, EUA.

Machado, R.T.H., 1988, “Modelagem e Simulação Numérica do Mecanismo de Gás-Lift Intermitente”, MSc. Dissertation, U.F. Ouro Preto, MG, Brazil.

Neely, A.B., Montgomery, J.W. and Vogel, J.V., 1974, “A Field Test and Analytical Study of Intermittent Gas Lift”, Trans. AIME 257, SPE Journal (SPE 4538), pp. 502-512.

Santos, O.G., Bordalo, S.N. and Alhanati, F.J.S., 2001, “Study of the dynamics, optimization and selection of intermittent gas-lift methods – a comprehensive model”, JPSE 32, pp. 231-248.

White, G.W. et al., 1963, “An Analytical Concept of the Static and Dynamic Parameters of Intermittent Gas Lift”, Trans. AIME 228, JPT, pp. 301-308.

Appendix A. Equation set of the IGL model

Table A.1. Variables of the IGL model.

i	y_i	Description
1	$\overline{\rho}_{gc}$	Average density of gas inside the casing annulus
2	ρ_{gc1}	Density of gas at the top of casing annulus
3	ρ_{gc2}	Density of gas at the bottom of casing annulus
4	P_{gc1}	Pressure of gas at the top of casing annulus
5	P_{gc2}	Pressure of gas at the bottom of casing annulus
6	$\overline{Z}_{gc}$	Average compressibility factor of gas inside the casing annulus
7	$\dot{m}_{gi}$	Mass flow rate of gas through the motor valve
8	$\overline{\rho}_{gt}$	Average density of the gas core inside the tubing
9	ρ_{gt1}	Density at the bottom of gas core inside the tubing
10	P_{gt1}	Pressure at the bottom of gas core inside the tubing
11	Z_{gt1}	Compressibility factor at the bottom of gas core inside the tubing
12	ρ_{gt2}	Density of gas at the top of gas core inside the tubing
13	P_{gt2}	Pressure at the top of gas core inside the tubing
14	Z_{gt2}	Compressibility factor at the top of gas core inside the tubing
15	z_{bt2}	Elevation of the top of gas core inside the tubing
16	v_{bt}	Velocity of the top of gas core inside the tubing
17	y_f	Average thickness of the liquid film on the tubing wall
18	z_{ft2}	Elevation of the top of liquid film on the tubing wall
19	v_{ft}	Average velocity of liquid film on the tubing wall
20	z_{st2}	Elevation of the top of slug inside the tubing
21	v_{st}	Average velocity of slug inside the tubing
22	z_{lt2}	Elevation of the top of liquid load inside the tubing
23	v_{lt}	Average velocity of the liquid load inside the tubing
24	$\dot{m}_{gv}$	Mass flow rate of gas through the GL valve
25	$\dot{m}_{lR}$	Mass flow rate of liquid from reservoir into the well bore

Table A.2. Ordinary differential equations of the IGL model.

$E(Y)$	$F(Y)$	
$\overline{\rho}_{gc}V_c$	$L_1\dot{m}_{gi} - L_2\dot{m}_{gv}$	(1.1)
$\overline{\rho}_{gt}A_b h_b$	$L_2\dot{m}_{gv} - L_6\dot{m}_{gp}$	(1.2)
$\rho_l A_f h_f$	$(L_4 \vee L_5)\rho_l v_{rsf} A_f - (L_6 \wedge v_f^+)\rho_l v_f A_f - L_7\rho_l v_{rfl} A_f + (\neg L_7 \wedge L_3)\dot{m}_{lR}$	(1.3)
$\rho_l A_t h_s$	$L_4\rho_l v_{rsf}, A_{f'} - (L_4 \vee L_5)\rho_l v_{rsf} A_f$	(1.4)
$\rho_l A_t h_s v_s$	$(P_{gt2} - P_{s2})A_t - \tau_{ts} S_{ts} - \rho_l g A_t h_s - L_5 K \rho_l \frac{v_s^2}{2} A_t$	(1.5)
z_{b2}	v_b	(1.6)
z_{s2}	v_s	(1.7)
$\rho_l A_t z_{l2}$	$\rho_l v_{rfl} A_f + L_3\dot{m}_{lR}$	(1.8)
z_{l2}	v_l	(1.9)

Table A.3. Algebraic equations and closure relations of the IGL model.

$G(Y)$			
$P_{c2} - P_{c1}\exp(\lambda h_c)$	(2.1)	$Z_{gt2} - \mathrm{Z}(P_{gt2r}, \overline{T}_{gtr}, Z_{gt2})$	(2.9)
$\overline{Z}_c - \mathrm{Z}(\overline{P}_{cr}, \overline{T}_{cr}, \overline{Z}_c)$	(2.2)	$\overline{\rho}_{gt} - (1-\alpha)\rho_{gt1} - \alpha\rho_{gt2}$	(2.10)
$\left(\frac{P}{\rho}\right)_{c1} - \frac{\overline{Z}_c \overline{R}\overline{T}_c}{M}$	(2.3)	$\left(\frac{P}{\rho}\right)_{gt1} - \frac{Z_{gt1}\overline{R}\overline{T}_{gt}}{M}$	(2.11)
$\left(\frac{P}{\rho}\right)_{c2} - \frac{\overline{Z}_c \overline{R}\overline{T}_c}{M}$	(2.4)	$\left(\frac{P}{\rho}\right)_{gt2} - \frac{Z_{gt2}\overline{R}\overline{T}_{gt}}{M}$	(2.12)
$\overline{\rho}_c - \rho_{c1}\frac{[\exp(\lambda h_c)-1]}{\lambda h_c}$	(2.5)	$z_{f2} - z_{b2}$	(2.13)
$\dot{m}_{gi} - \rho_{gsc}\frac{1{,}5136\times10^{-6} C_v P_{gi}}{\sqrt{d_g T_S}}\sqrt{\frac{P_{gc1}}{P_{gi}} - \left(\frac{P_{gc1}}{P_{gi}}\right)^2}$	(2.6)[a]	$(P_{gt1} - P_{gt2})A_f + \tau_{fb}S_{fb} - \tau_{tf}S_{tf} - \rho_l g A_f h_f$	(2.14)
$(P_{gt1} - P_{gt2})A_b - \tau_{fb}S_{fb} - \overline{\rho}_{gt} g A_b h_b$	(2.7)	$\dot{m}_{lR} - \rho_l IP(P_R - P_{wf})$	(2.15)
$Z_{gt1} - \mathrm{Z}(P_{gt1r}, \overline{T}_{gtr}, Z_{gt1})$	(2.8)		
$\dot{m}_{gv} - \rho_{gsc}\frac{4{,}842\times10^{-2} C_d A_{gv} P_{gc2}}{\sqrt{d_g T_{gv}}}\sqrt{2\left(\frac{k}{k-1}\right)\left[\left(\frac{P_{t1}}{P_{gc2}}\right)^{2/k} - \left(\frac{P_{t1}}{P_{gc2}}\right)^{(k+1)/k}\right]}$			(2.16)[a]

$h_c = z_{wh} - z_{gv}$	$V_c = \frac{\pi}{4}(D_c^2 - D_t^2)h_c$	$\overline{P}_{gc} = \overline{\rho}_{gc}\frac{\overline{Z}_{gc}\overline{R}\overline{T}_{gc}}{M}$	$\overline{T}_{gc} = \frac{T_S + T_{gv}}{2}$
$T_z = T_S + g_G(z_{wh} - z)$	$\lambda = \frac{Mg}{\overline{Z}_g \overline{R}\overline{T}_g}$	$h_b = z_{b2} - z_{b1}$	$A_b = \frac{\pi}{4}(D_t - 2y_f)^2$
$S_{fb} = \pi(D_t - 2y_f)h_b$	$\tau_{fb} = C_{f_{fb}}\overline{\rho}_{gt}\frac{v_{rfb}^2}{2}$	$\overline{T}_{gt} = \frac{\overline{T}_{gc} + T_R}{2}$	$h_f = z_{f2} - z_{f1}$
$v_{rsf} = v_b - v_f$	$v_{rsf'} = v_b - v_{f'}$	$v_{rfl} = v_f - v_l$	$A_f = \pi y_f(D_t - y_f)$
$S_{tf} = \pi D_t h_f$	$\tau_{tf} = C_{f_{tf}}\rho_l\frac{v_f^2}{2}$	$h_s = z_{s2} - z_{b2}$	$P_{s2} = P_{wh}\exp[\lambda(z_{wh} - z_{s2})]$
$A_t = \frac{\pi}{4}D_t^2$	$S_{ts} = \pi D_t h_s$	$\tau_{ts} = C_{f_{ts}}\rho_l\frac{v_s^2}{2}$	$P_{wf} = P_{gt1} + \rho_l g z_{l2}$

[a] - expressions in SI units.

Appendix B. Controls for the simultaneous and coupled simulation scheme

Table B.1. Logical flags (L) and operators for simulation control.

i	L_i
1	Motor valve control
2	Gas-Lift valve control
3	Check valve control
4	Elevation stage control
5	Production stage control
6	Decompression stage control
7	Loading stage control
$\vee$ - or	$\wedge$ - and $\neg$ - not

Table B.2. Controls for motor valve during IGL operation.

Status	Condition	Var's, Eq's & Flags
Open	$t > (n_{inj} - 1)\Delta t_{ciclo}$	Var.7, Eq.(2.6) , $L_1 = 1$
Closed	$t \geq (n_{inj} - 1)\Delta t_{ciclo} + \Delta t_{inj}$	$L_1 = 0$

Table B.3. Controls for GL valve during IGL operation.

Status	Condition	Var's, Eq's & Flags
Open	$P_{gc2} > \dfrac{P_{gv} - RP_{t1}}{1 - R}$	Var.24, Eq.(2.16) , $L_2 = 1$
Closed	$P_{gc2} \leq P_{gv}$	$L_2 = 0$

Table B.4. Controls for check valve during IGL operation.

Status	Condition	Var's, Eq's & Flags
Open	$P_R + \rho_l g z_{gv} > P_{t1}$	Var.25, Eq.(2.15) , $L_3 = 1$
Closed	$P_R + \rho_l g z_{gv} \leq P_{t1}$	$L_3 = 0$

Table B.5. Simulation procedure for IGL model.

Stage	Start	End	Var's, Eq's & Flags
Injection	motor valve opens	motor valve closes	Var.1-6; Eq.(1.1), Eq.(2.1-5); $L_1 = 1$
Elevation	GL valve opens	The top of the slug reaches the well head	Var.8-21; Eq.(1.2-7), Eq.(2.7-14); $L_4 = 1$, $L_6 = L_7 = 0$
Production	The top of the slug reaches the well head	The base of the slug reaches the well head	Var.8-19,21; Eq.(1.2-6), Eq.(2.7-14); $L_4 = 0$, $L_5 = 1$
Decompression	The base of the slug reaches the well head	The average gas pressure into the tubing becomes equal to the wellhead pressure	Var.8-11,16-17,19; Eq.(1.2-3), Eq.(2.7-8,10, 12,14); $L_5 = 0$, $L_6 = 1$
Loading	GL valve closes while check valve stands open	GL valve opens for another IGL cycle	Var. 22-23; Eq.(1.8-9); $L_7 = 1$